Transformation to Nanocrystallites in Amorphous Alloys Induced by Resonant Electropulsing

Ting Hao[*1], Hisanori Tanimoto and Hiroshi Mizubayashi[*2]

Institute of Materials Science, University of Tsukuba, Tsukuba 305-8573, Japan

The electropulsing-induced low temperature crystallization (*e*-LTC) of marginal amorphous (*a*-) alloys, *a*-$Cu_{50}Ti_{50}$ and *a*-$Pd_{80}Si_{20}$, and a bulk amorphous alloy, *a*-$Zr_{60}Cu_{30}Al_{10}$, was investigated by electropulsing at room temperature (*RT*) and in liquid nitrogen (LN₂). Electropulsing was made by means of discharge of a condenser which is characterized by the initial current density, i_{d0}, and the decay time, τ, where the frequency of the principal constituent Fourier component of the electropulsing is $1/2\pi\tau$. The range of i_{d0} was between 10^8 and 10^{10} A/m² and that of τ was between 0.1 and 20 ms. For all the amorphous alloys, the *e*-LTC took place during single electropulsing with i_{d0} beyond the threshold current density, $i_{d0,c}$, where $i_{d0,c}$ was a function of τ. The maximum specimen temperature during the *e*-LTC was, *e.g.*, 200 K for electropulsing in LN₂, indicating that the *e*-LTC is associated with an athermal process, the resonant collective motion of the relatively high density region here. The dependence of $i_{d0,c}$ on τ found for electropulsing in LN₂ showed good agreement with that observed at *RT*, indicating that the density fluctuation responsible for the *e*-LTC was that frozen at the glass transition temperature. The transmission electron microscopy observation revealed that crystallites formed by the *e*-LTC showed crystallographic alignment with each other, suggesting that the transformation of the relatively high density regions to a crystalline phase took place. The underlying mechanism of the *e*-LTC was discussed.

1. Introduction

After finding of acceleration of thermal crystallization in amorphous alloys by an electric current,[1,2] many works have been done to get insight into the underlying mechanism.[3] For amorphous (*a*-) $Cu_{50}Ti_{50}$, *a*-$Cu_{50}Zr_{50}$ and *a*-$(Zr_{70}$-$Cu_{30})_{92.5}Al_{7.5}$, an electric direct-current of 10^7 A/m² caused a decrease in the crystallization temperature, T_x, by 10 to 20 K and the enhancement of the homogeneous nucleation process was observed.[4–7] Since the effective charge number to explain such enhancement of atomic diffusion by the electromigration force induced at an electric direct-current of 10^7 A/m² was the order of 10^6, the concentration of the electromigration force through a collective motion of many atoms was claimed to enhance atomic diffusion.[4–7] For Fe–Si–B amorphous alloys, repetition of electric square pulses of 10^9 A/m² with about 0.1 ms duration for one hour, a total of a few seconds for passing current, brought about a decrease in the crystallization temperature by 150 to 170 K, where enhancement of atomic diffusion by the stochastic resonance was claimed to take place.[8,9] That is, the concentration of the electromigration force through a collective motion of many atoms is claimed too. These findings stimulated theoretical works on the influence of an electric current[10,11] or an electric field[12] on the phase transformation in the light of thermodynamics. However, the underlying mechanism for the enhancement of atomic diffusion or atomic motion, *i.e.*, the relationship between the characteristic effects of passing electric current and the probable collective motion of many atoms in amorphous alloys is not known yet.

Meanwhile, in order to get insight into a collective motion of many atoms in amorphous alloys, the dynamic Young's modulus was investigated as a function of measurement frequencies for *a*-$Pd_{80}Si_{20}$, *a*-$Cu_{50}Ti_{50}$, *a*-$Cu_{50}Zr_{50}$ and *a*-$Zr_{60}Cu_{30}Al_{10}$.[13,14] In the frequency range between 10^2 and 10^4 Hz studied, the dynamic Young's modulus measured with the strain amplitude of 10^{-6} showed much lower values than the static Young's modulus measured by tensile tests, indicating that a resonant anelastic process was excited. It was further found that the dynamic Young's modulus at around 10^2 Hz increased beyond the static Young's modulus[14] when the strain amplitude was increased from 10^{-6} to 10^{-3}.

It is known that the static Young's modulus in amorphous alloys is lower by 20 to 40% than that in the corresponding crystalline alloys, where a localized shear deformation in the relatively lower density region is responsible for the decrease in the Young's modulus.[15,16] It is further reported that the localized shear deformation shows saturation with increasing applied strain as the bond switching is completed.[17] Then one may elucidate that at a low strain amplitude, a resonant collective motion of many atoms causes the localized shear deformation of surrounding atoms which brings about the decrease in the dynamic Young's modulus. On the other hand, at a high strain amplitude, the dynamic Young's modulus shows an increase because of saturation of the localized shear deformation of surrounding atoms. After the consideration, one may expect that the dynamic Young's modulus at a low strain amplitude shows an increase by an electric current instead of an increase in the strain amplitude because an electric direct-current may induce the internal stress due to the concentration of electromigration force associated with a collective motion of many atoms. Experimentally, it was observed for *a*-$Cu_{50}Ti_{50}$,[6,18] *a*-$Cu_{50}Zr_{50}$,[7,18] *a*-$Pd_{80}Si_{20}$,[18] *a*-$(Zr_{70}Cu_{30})_{92.5}Al_{7.5}$[18] and *a*-$Zr_{60}Cu_{30}Al_{10}$[19] that the dynamic Young's modulus at the strain amplitude of 10^{-6} and around 10^2 Hz showed an increase by passing an electric direct-current of 10^7 A/m². We assumed that the increase in the dynamic Young's modulus by the electric direct-current is caused by the internal stress due to the

---
[*1]Graduate Student, University of Tsukuba, Present address: Institute for Materials Research, Tohoku University, Sendai 980-8577, Japan
[*2]Corresponding author, E-mail: mizuh@ims.tsukuba.ac.jp

concentration of electromigration force associated with a collective motion of many atoms. The effective charge number, Z^*, to explain the concentration of electromigration force was the order of 10^5 for various amorphous alloys.[6,7,18,19)] It is noted that for the electromigration effect, the value of Z^* is larger by four to five digits than the effective charge number, z^*, of a single atom in a concentrated alloy.[20)] A model to explain the effect of passing electric current on the dynamic Young's modulus is as follows: The concentration of the electromigration force associated with a collective motion of many atoms causes a decrease in the motional amplitude of its resonant motion excited by elastic vibrations because of saturation of the localized shear deformation of surrounding atoms. If it is the case, one can expect that a resonant collective motion of many atoms can be excited by resonant electropulsing.

Such resonant electropulsing can be made by means of discharge of a condenser. During electropulsing, the current density, i_d, decays with increasing elapsed time, t, as,

$$i_d = i_{d0} \exp(-t/\tau), \tag{1}$$

where i_{d0} is the initial value of i_d and τ is the decay time of discharge. It is noted that the frequency of the principal Fourier constituent of (1) is $1/2\pi\tau$, i.e., $1/2\pi\tau$ may be tuned to excite a resonant collective motion by adjusting τ. Experimentally, it was found for a-$Cu_{50}Ti_{50}$ and a-$Pd_{80}Si_{20}$ that the crystallization took place during single electropulsing with τ of about 1 ms below 400 K when i_{d0} was higher than the threshold value.[21)] That is, electropulsing induces the low-temperature crystallization (e-LTC, hereafter).

On the other hand, it was reported for several bulk metallic glasses that ultrasound induced the rapid crystallization around the glass transition temperature, T_g, where enhancement of atomic diffusion by the stochastic resonance was claimed to take place.[22–24)] As already mentioned, the decrease in the crystallization temperature by repetition of electric square pulses for one hour was also claimed to be associated with the stochastic enhancement of atomic diffusion.[8,9)] In contrast, a distinguishing characteristics of the e-LTC due to electropulsing is the crystallization for 1 ms below 400 K[21)] which may not be explained by the stochastic enhancement of atomic diffusion because rapid cool-down and enhancement of atomic diffusion for 1 ms correspond to quenching into the amorphous state. In order to clarify this issue further, electropulsing was carried out for a-Zr_{60}-$Cu_{30}Al_{10}$ in a liquid nitrogen (LN_2) bath to minimize an effect of thermal agitation for atomic diffusion. It is noted that a-$Zr_{60}Cu_{30}Al_{10}$ is known as a bulk amorphous alloy showing (T_x–T_g) of about 80 K at a heating rate of 0.4 K/s.[25)] For marginal amorphous alloys, electropulsing was also carried out for a-$Cu_{50}Ti_{50}$ and a-$Pd_{80}Si_{20}$ in a liquid nitrogen (LN_2) bath. The transmission electron microscope (TEM) observations were made to investigate the microstructures after the e-LTC.

2. Experiment

Thin tapes of a-$Cu_{50}Ti_{50}$, and a-$Pd_{80}Si_{20}$ and a-Zr_{60}-$Cu_{30}Al_{10}$ were prepared by melt spinning in a high-purity Ar gas atmosphere. Both surfaces of a tape specimen were smoothed by polishing mechanically using fine emery paper in water avoiding heat-up during polishing. The thickness and width of specimens after polishing were about 20 μm and 0.8 mm for a-$Cu_{50}Ti_{50}$ specimens, about 25 μm and 0.9 mm for a-$Pd_{80}Si_{20}$ specimens and about 30 μm and 0.9 mm for a-$Zr_{60}Cu_{30}Al_{10}$ specimens, respectively. The specimen setup for electropulsing was similar to that reported in the previous work.[21)] A specimen was sandwiched by two aluminum nitride (AlN)/boron nitride (BN)-composite substrates with the thermal conductivity of 90 W·K^{-1}·m^{-1} to minimize an effect of joule heating during electropulsing, where τ, i_{d0} and the electric energy of single electropulsing given to the unit volume of a specimen, P_d, were estimated as follows. A condenser with the capacitance C was charged to the terminal voltage, V_0, and then discharge for electropulsing was made, where the circuit resistivity, $R_{circuit}$, was composed of the resistivity of wiring, R_{wiring}, and that of a specimen between current-terminals, $R_{specimen}$. τ, i_{d0} and P_d were estimated as $CR_{circuit}$, $(V_0/R_{circuit})/S_s$ and $(CV_0^2/2) \times (R_{specimen}/R_{circuit})/v_s$, respectively, where v_s and S_s denote the specimen volume between the current-terminals and the section area of a specimen, respectively. The electric resistivity of a specimen, R, was measured before and after each electropulsing to monitor the e-LTC. Electropulsing experiments were carried out at RT and in a LN_2 bath. The X-ray diffraction (XRD) measurements were made by the θ–2θ scan using the Cu-K_α radiation, where reflections from Si powder put on a specimen surface were used as reference. The microstructure of a specimen was investigated by the TEM, JEOL 2010, operated at 200 kV. Thinning of a specimen was made by electrochemical polishing for a-$Cu_{50}Ti_{50}$ or by focused ion beam thinning for a-$Pd_{80}Si_{20}$ and a-$Zr_{60}Cu_{30}Al_{10}$, respectively.

3. Results

3.1　a-$Cu_{50}Ti_{50}$

Figure 1(a) shows an example of resistivity changes in an a-$Cu_{50}Ti_{50}$ specimen observed after electropulsing with $\tau = 1.0$ ms in LN_2, where the resistivity was measured at 78 K in LN_2. In Fig. 1(a), the normalized resistivity, R/R_0, is plotted against P_d (the bottom horizontal axis) and also against i_{d0} (the upper horizontal axis), where R_0 denotes the resistivity of a virgin specimen. It is noted that each data point was observed after single electropulsing. The e-LTC started when i_{d0} increased beyond the threshold value, $i_{d0,c}$. It is noted that virgin electropulsing can induce the e-LTC when i_{d0} is higher than $i_{d0,c}$. In the present work, i_{d0} was increased sequentially from a low value in order to find $i_{d0,c}$. In Fig. 1(a) for $\tau = 1.0$ ms, $i_{d0,c}$ was 1.7×10^9 A/m^2 which corresponded to P_d of 2.6 J/mm^3.

Figure 1(b) shows examples of the specimen temperature, T, vs. elapsed time, t, data observed for electropulsing with $\tau = 1.0$ ms, where the theoretical T vs. t curve for P_d of 2.6 J/mm^3 is also shown. The theoretical T vs. t curve was estimated for a 20 μm thick specimen sandwiched by two AlN/BN-composite substrates, where the thermal conductivity used was 90 W·K^{-1}·m^{-1} for the AlN/BN-composite substrate and 1 W·K^{-1}·m^{-1} for a-$Cu_{50}Ti_{50}$. It is reported[26)] that the thermal conductivity of a-$Zr_{55}Cu_{30}Al_{10}Ni_5$ at 80 K is
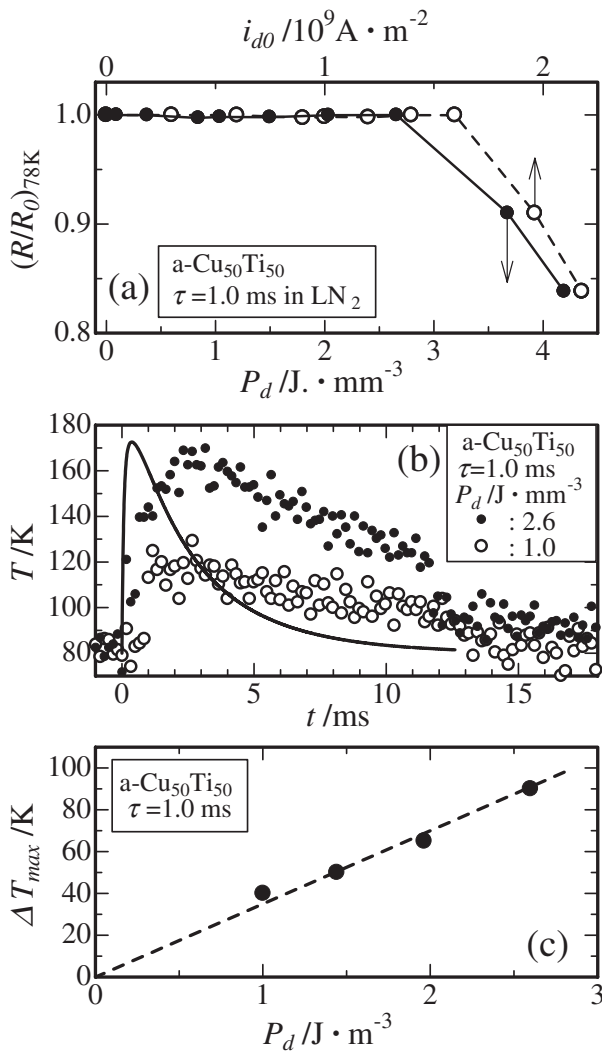
Fig. 1 (a) Changes in R at 78 K observed for an a-Cu$_{50}$Ti$_{50}$ specimen after resonant-electropulsing with $\tau = 1.0$ ms in LN$_2$. (b) Changes in T observed during resonant-electropulsing with $\tau = 1.0$ ms and $P_d = 2.6$ J/mm^3 or $P_d = 1.0$ J/mm^3. The solid curve denotes the theoretical time evolution of T for $P_d = 2.6$ J/mm^3 (see text for details). (c) The ΔT_{max} vs. P_d data observed for resonant-electropulsing with $\tau = 1.0$ ms in LN$_2$ (see text for ΔT_{max}). The dashed line is drawn to guide eyes.

Fig. 2 (a) Examples of the R/R_0 vs. i_{d0} plot observed for electropulsing with various τ at RT, where the data for $\tau \sim 2$ ms, ~ 1 ms and ~ 0.2 ms reported[21] are shown together. (b) Examples of the R/R_0 vs. i_{d0} plot observed for electropulsing in LN$_2$.

estimated to be $2 \, \text{W} \cdot \text{K}^{-1} \cdot \text{m}^{-1}$. The assumptions of good thermal contact between the AlN/BN-composite substrate and an a-Cu$_{50}$Ti$_{50}$ specimen and the thermal conductivity of a-Cu$_{50}$Ti$_{50}$ to be $2 \, \text{W} \cdot \text{K}^{-1} \cdot \text{m}^{-1}$ give an increase in the specimen temperature being much lower than that observed. Then we assumed that the effective thermal conductivity of a-Cu$_{50}$Ti$_{50}$ decreases to one half of $2 \, \text{W} \cdot \text{K}^{-1} \cdot \text{m}^{-1}$ because of not perfect thermal contact between the AlN/BN-composite substrate and an a-Cu$_{50}$Ti$_{50}$ specimen. In Fig. 1(b), the theoretical temperature of the middle of the specimen thickness is compared with the temperature observed at the specimen surface. It is noted that for the specimen setup oriented for the temperature measurements,[21] the specimen surface around the contact point to the thin thermocouple faces to resin but not to AlN/BN composite substrate. Therefore the observed temperature is expected to be higher than the maximum temperature attained in a specimen in the specimen setup without a thermocouple. After the start of
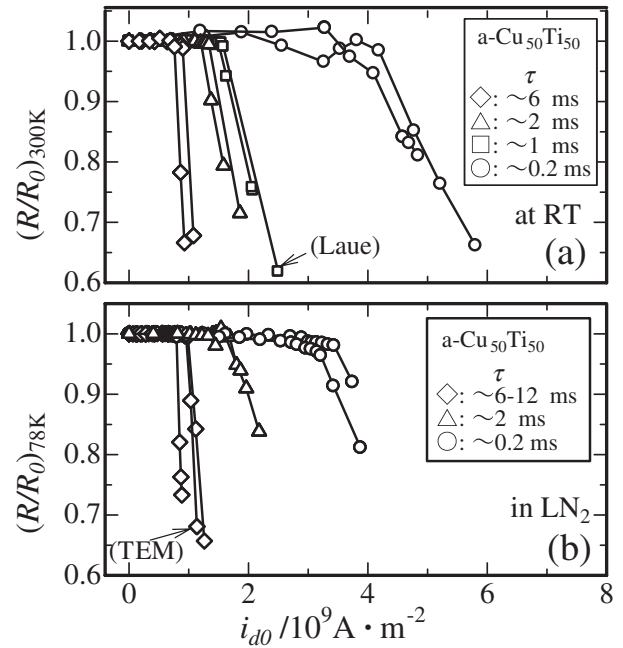
electropulsing, the theoretical T vs. t curve shows a steep increase because of nearly adiabatic heating at first which is followed by the maximum and subsequent gradual decrease due to thermal flow to the AlN/BN composite substrate. On the other hand, the observed temperature increased to the maximum temperature, T_{max}, in a few milliseconds and then decreased in a few ten milliseconds. Such delayed responses were associated with the specimen setup oriented for the temperature measurements mentioned above.

In Fig. 1(c), the maximum increase in the specimen temperature, ΔT_{max}, observed for the specimen shown in Fig. 1(b) is plotted against P_d, where ΔT_{max} increased linearly with P_d. The observed results shown in Figs. 1(a) to (c) indicate that the e-LTC in LN$_2$ took place below 200 K for a few milliseconds where a considerable volume fraction of the specimen was crystallized. It is not shown here but the nose temperature found in the time-temperature-transformation (TTT) diagram for a-Cu$_{50}$Ti$_{50}$[21] is 855 K at the elapsed time of 0.26 s and the T vs. t data plotted on the TTT diagram indicates that no thermal crystallization was expected during the present electropulsing.

Figures 2(a) and (b) show examples of resistivity changes in a-Cu$_{50}$Ti$_{50}$ specimens observed after electropulsing with various τ at RT and those in LN$_2$, respectively. As seen in Figs. 2(a) and (b), $i_{d0,c}$ for the e-LTC showed a decrease with increasing τ, which might be associated with the increase in the effective charge number, Z^*, for the collective motion under passing electric current (not shown here). The maximum decrease of R/R_0 associated with the e-LTC due to single electropulsing at RT was 0.5 in $|\Delta R/R_0|_{r\text{-}e}/|\Delta R/R_0|_x$, where the decrease in R at RT observed after the thermal crystallization at elevated temperatures, $(\Delta R/R_0)_x$, was -0.8 for a-Cu$_{50}$Ti$_{50}$.[21]
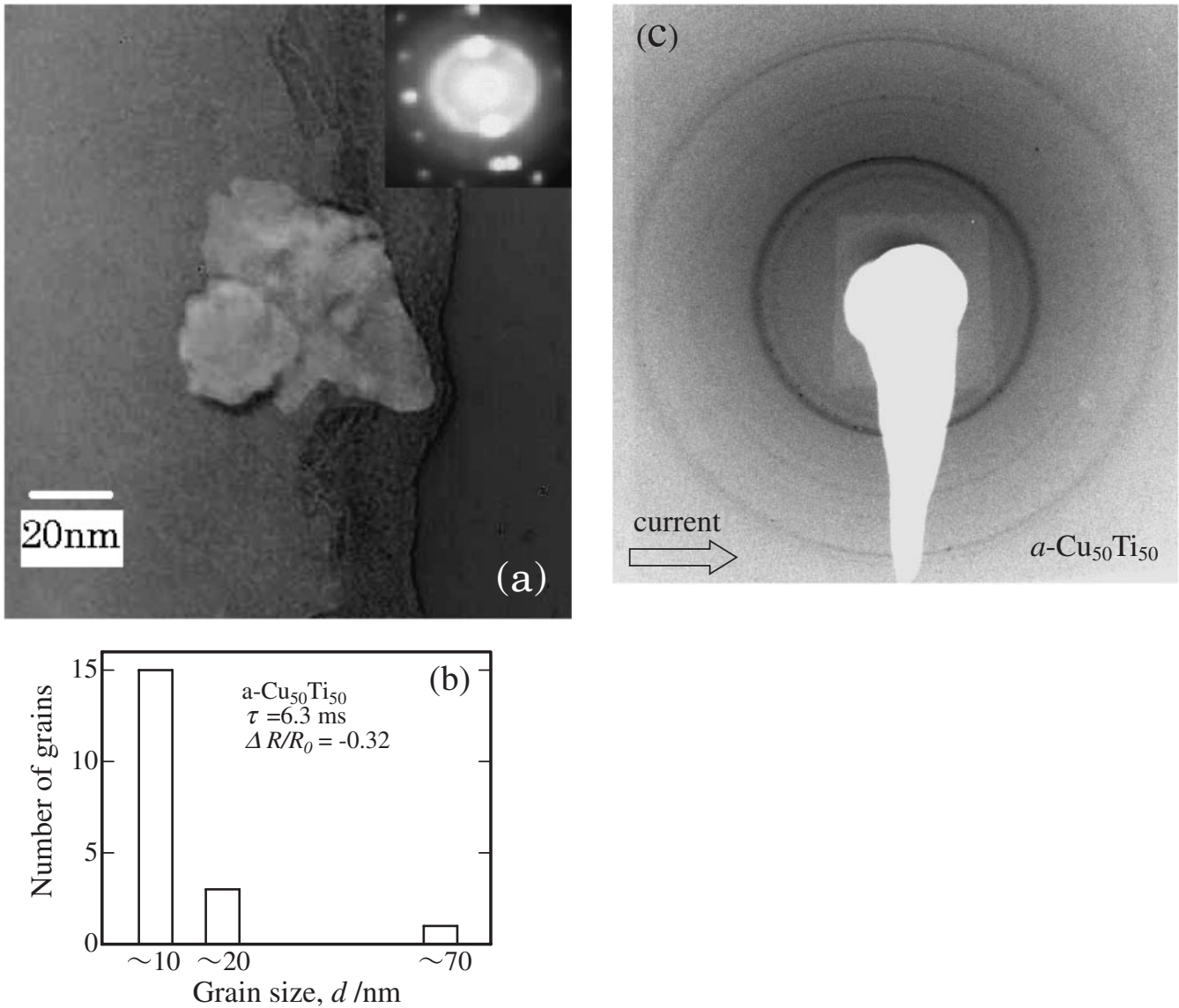
The crystalline phase observed after the thermal crystal-

Fig. 3 (a) The TEM image and (b) grain size distribution observed for the a-$Cu_{50}Ti_{50}$ specimen which showed $\Delta R/R_0$ of -0.32 due to electropulsing with $\tau = 6.3$ ms in LN_2 [see Fig. 2(b)]. (c) The XRD Laue pattern observed for the a-$Cu_{50}Ti_{50}$ specimen which showed $\Delta R/R_0$ of -0.38 due to single electropulsing with $\tau = 0.6$ ms at RT [see Fig. 2(a)]. The white area seen in (c) are of extrinsic origin due to the imaging plate used.

lization and that found after the e-LTC were always crystalline (c-) CuTi for electropulsing at RT and electropulsing in LN_2 (not shown here). Figure 3(a) is a TEM image observed for the a-$Cu_{50}Ti_{50}$ specimen which showed $\Delta R/R_0$ of -0.32 after the e-LTC in LN_2 [see Fig. 2(b)], where two crystallites with the grain size of about 20 and 70 nm can be seen. The inset is the selected area diffraction (SAD) pattern of the area shown in Fig. 3(a), indicating that crystallographic directions of crystallites showed good alignment. Figure 3(b) is the grain size distribution observed for the a-$Cu_{50}Ti_{50}$ specimen, where the grain size was about 10 nm for most crystallites and a crystallite with the grain size of about 70 nm was found too. Figure 3(c) shows the XRD Laue pattern observed for the a-$Cu_{50}Ti_{50}$ specimen which showed $\Delta R/R_0$ of -0.38 due to single electropulsing with $\tau = 0.6$ ms at RT [see Fig. 2(a)]. In Fig. 3(c), Debye rings and several fine XRD spots can be seen. Since Debye rings were broad, the most crystallites were very fine. The width of Debye rings

is a function of the direction of electric current, $i.e.$, the width of the upper and lower parts is wider than that of the right and left parts.

In Fig. 4(a), $i_{d0,c}$ was plotted against τ. The $i_{d0,c}$ $vs.$ τ data observed for electropulsing in LN_2 showed good agreement with those observed at RT. It is seen in Fig. 4(a) that $i_{d0,c}$ showed a tendency of decrease with increasing τ accompanied with shallow local minima depicted as the curves 1 to 3. Figure 4(b) shows the dynamic Young's modulus, E_d, as a function of $1/2\pi f$ and the static Young's modulus, E_s, as reference, where E_d was observed at RT with the strain amplitude of 10^{-6} without electric current, f was the vibration frequency of a specimen and E_s was observed in the tensile test at RT. In the $1/2\pi f$ range between 0.05 and 10 ms, E_d was considerably lower than E_s, where the curve 4 was fitted to the E_d $vs.$ f data. The curves 1 to 4 will be mentioned later.
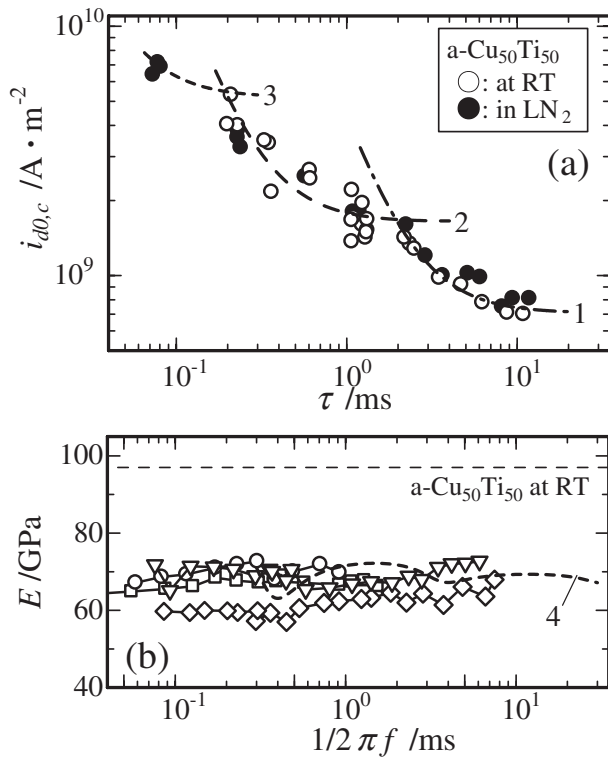
Fig. 4 (a) The $i_{d0,c}$ vs. τ data observed for electropulsing at RT and those observed for electropulsing in LN_2, where the data at RT reported for τ shorter than 3 ms[21] are shown too. (b) The E_d vs. f data observed at RT for four specimens. The dashed line denotes E_s. See text for the curves 1 to 4.
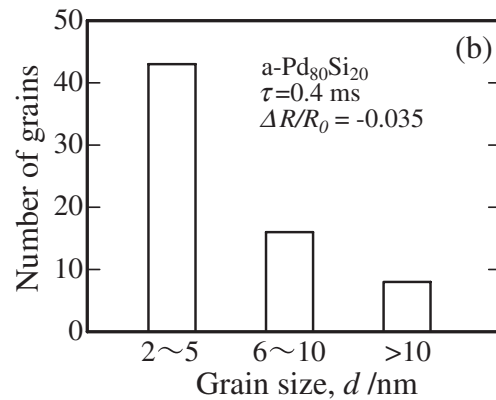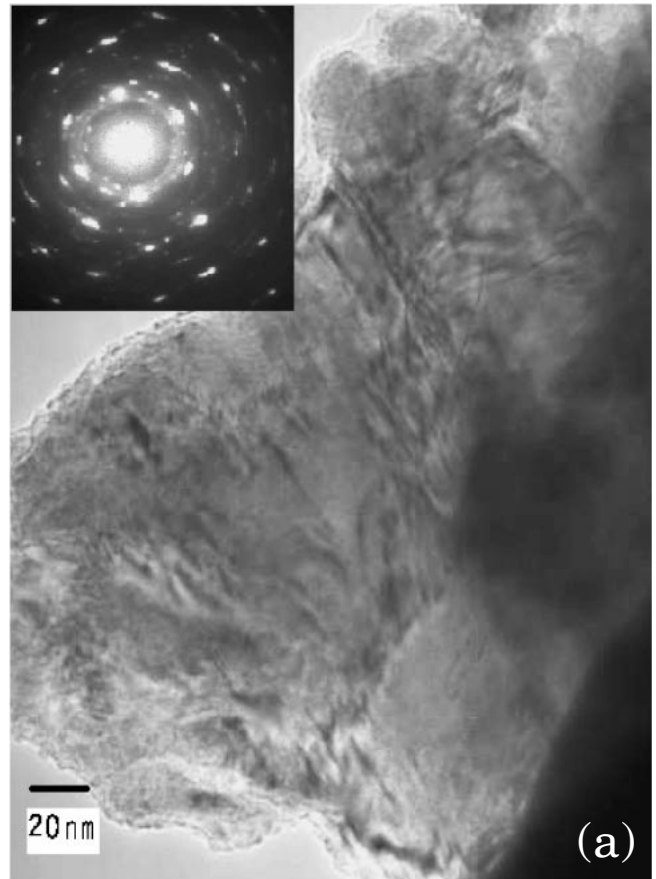

Fig. 5 (a) Examples of the R/R_0 vs. i_{d0} plot observed for electropulsing with various τ at RT, where the data for $\tau \sim 1.4$ ms, ~ 0.5 and ~ 0.2 ms reported[21] are shown together. (b) Example of the R/R_0 vs. i_{d0} plot observed for electropulsing in LN_2.

3.2 a-Pd$_{80}$Si$_{20}$

Figures 5(a) and (b) are similar to Figs. 2(a) and (b), respectively, but here the data observed for a-Pd$_{80}$Si$_{20}$ are shown. T_{max} observed for electropulsing with $i_{d0,c}$ in LN_2 was

Fig. 6 (a) A TEM image and (b) grain size distribution observed for a-Pd$_{80}$Si$_{20}$ specimen which showed $\Delta R/R_0$ of -0.035 due to single electropulsing with $\tau = 0.4$ ms in LN_2 [see Fig. 5(b)].
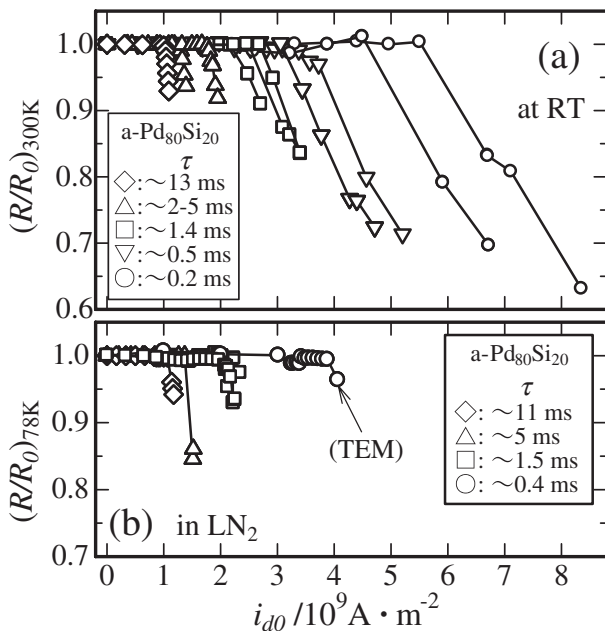
considerably lower than RT (not shown here). See Ref. 21) for T_{max} observed for electropulsing at RT and the TTT diagram for a-Pd$_{80}$Si$_{20}$. The maximum decrease in R/R_0 associated with the e-LTC during single electropulsing was 0.35 in $|\Delta R/R_0|_{r-e}/|\Delta R/R_0|_x$ as seen in Fig. 5(a), where $(\Delta R/R_0)_x$ was -0.6 for a-Pd$_{80}$Si$_{20}$.[21] It is not shown here but the XRD spectra observed after the e-LTC in LN_2 are very similar to those observed after the e-LTC at RT.[21]

Figure 6(a) is a TEM image observed for the a-Pd$_{80}$Si$_{20}$ specimen which showed $(\Delta R/R_0)_{r-e}$ of -0.035 due to single electropulsing in LN_2 [see Fig. 5(b)]. The SAD pattern indicates that crystallographic directions of the most crystallites showed good alignment among the crystallites. Figure 6(b) is the grain size distribution observed for the
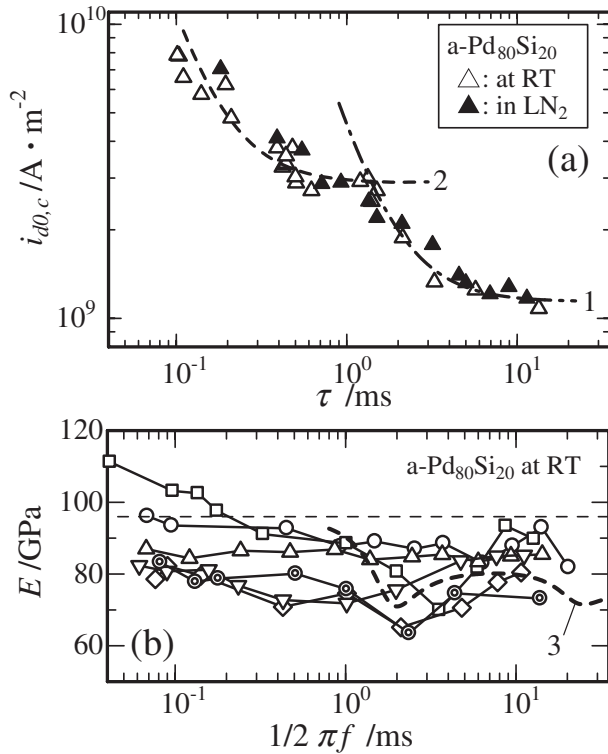
Fig. 7 (a) The $i_{d0,c}$ vs. τ data observed for electropulsing at *RT* and those observed for electropulsing in LN$_2$, where the data at *RT* reported for τ shorter than 3 ms[21] are shown too. (b) The E_d vs. f data reported for a-Pd$_{80}$Si$_{20}$ at *RT*.[13,14] The dashed line denotes E_s. See text for the curves 1 to 3.

Fig. 8 (a) An example of the R/R_0 vs. i_{d0} plot observed for electropulsing with various τ at *RT*, where the data for $\tau \leq 2$ ms reported[26] are shown together. (b) An example of the R/R_0 vs. i_{d0} plot observed for electropulsing with various τ in LN$_2$.

a-Pd$_{80}$Si$_{20}$ specimen, where the grain size was 2 to 5 nm for most of crystallites and crystallites with grain size beyond 10 nm were a few. The outline of the XRD Laue pattern observed for the a-Pd$_{80}$Si$_{20}$ after the e-LTC were similar to that mentioned in Fig. 3(c) except that no visible XRD spots were observed (not shown here).

Figures 7(a) and (b) are similar to Fig. 4(a) and (b), respectively, but here the data observed for a-Pd$_{80}$Si$_{20}$ are shown. In Fig. 7(a), $i_{d0,c}$ showed the trendency of decrease with increasing τ accompanied with the shallow minima depicted as the curves 1 and 2. The dependence of $i_{d0,c}$ on τ observed for electropulsing in LN$_2$ was very similar to that for electropulsing at *RT*. The curves 1 to 3 will be mentioned later.

3.3 a-Zr$_{60}$Cu$_{30}$Al$_{10}$

Figures 8(a) and (b) are similar to Figs. 2(a) and (b), respectively, but here the data observed for a-Zr$_{60}$Cu$_{30}$Al$_{10}$ are shown. T_{max} observed for electropulsing with $i_{d0,c}$ in LN$_2$ was considerably lower than *RT* (not shown here). See Ref. 27) for T_{max} observed for electropulsing at *RT* and the TTT diagram for a-Zr$_{60}$Cu$_{30}$Al$_{10}$. The maximum decrease in $|\Delta R/R_0|_{r-e}/|\Delta R/R_0|_x$ after the e-LTC due to single electropulsing was 0.05 as seen in Figs. 8(a) and (b) where $(\Delta R/R_0)_x$ is -0.5 for a-Zr$_{60}$Cu$_{30}$Al$_{10}$ at *RT*. The sign of changes in R were a function of τ, where R showed an increase for τ between 2 ms and 6 ms and a decrease for $\tau > 6$ ms and $\tau < 2$ ms. The relationship between $(\Delta R/R_0)_{r-e}$ vs. i_{d0} and that between $(\Delta R/R_0)_{r-e}$ vs. τ found for electro-
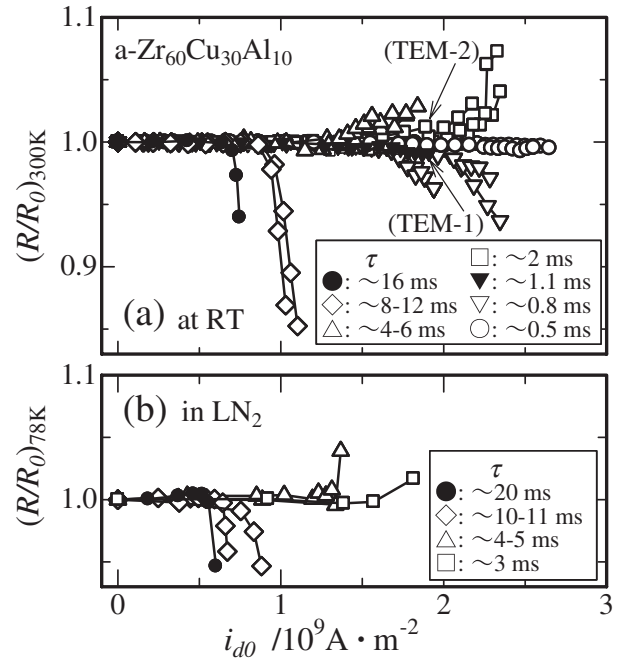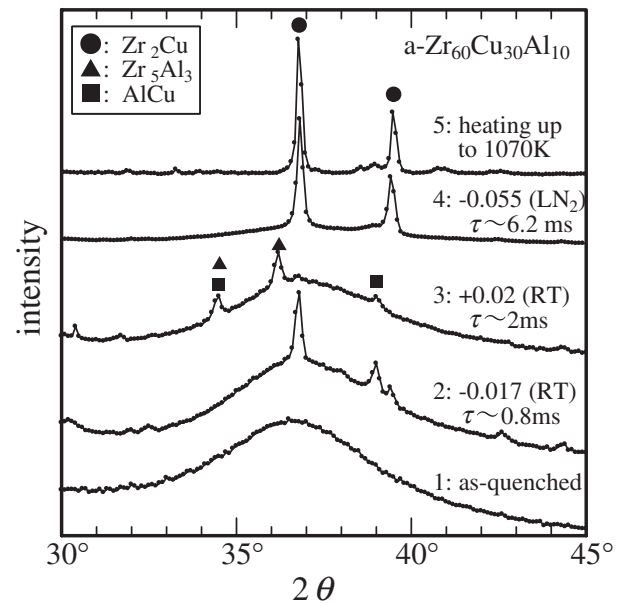

Fig. 9 XRD spectra observed in a-Zr$_{60}$Cu$_{30}$Al$_{10}$ specimens. 1: as quenched, 2: $\Delta R/R_0 = -0.017$ due to electropulsing with $\tau \sim 0.8$ ms at *RT*, 3: $\Delta R/R_0 = +0.02$ due to electropulsing with $\tau \sim 2$ ms at *RT*, 4: $\Delta R/R_0 = -0.055$ due to electropulsing with $\tau \sim 6.2$ ms in LN$_2$, 5: annealed at 1070 K without electropulsing. The data 1, 2 and 5 were reported in Ref. 27).

pulsing in LN$_2$ were similar to those observed for electropulsing at *RT*.

Figure 9 shows the XRD spectra observed in a-Zr$_{60}$-Cu$_{30}$Al$_{10}$ specimens. The XRD spectrum observed after annealing at 1070 K is similar to that reported for a-Zr$_{60}$-Cu$_{30}$Al$_{10}$ after annealing at elevated temperature, where

Fig. 10   (a) TEM image and (b) grain size distribution observed for the a-$Zr_{60}Cu_{30}Al_{10}$ specimen which showed $\Delta R/R_0$ of -0.01 due to electropulsing at RT [see TEM-1 in Fig. 8(a)].
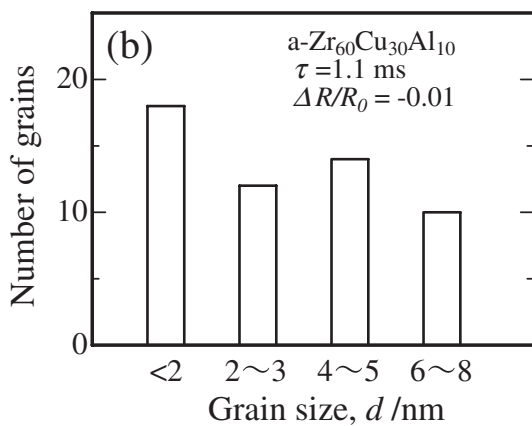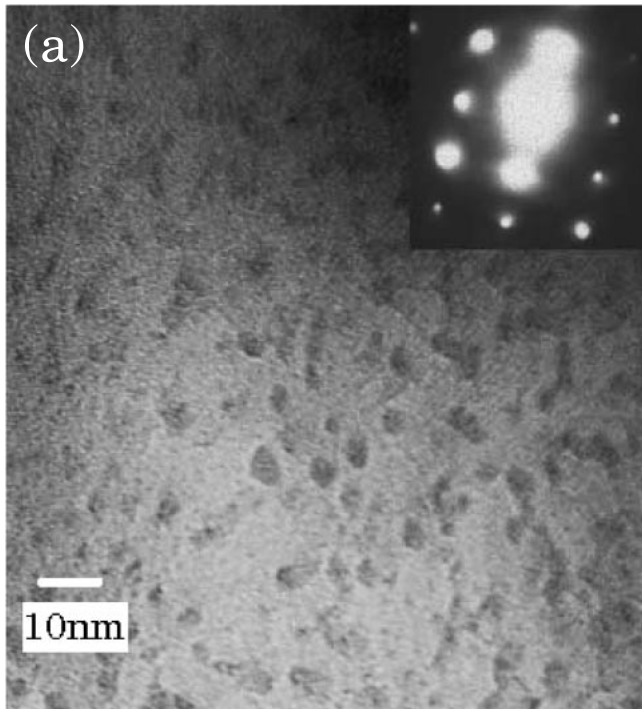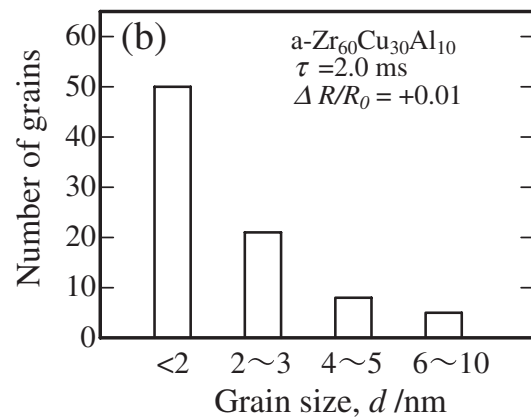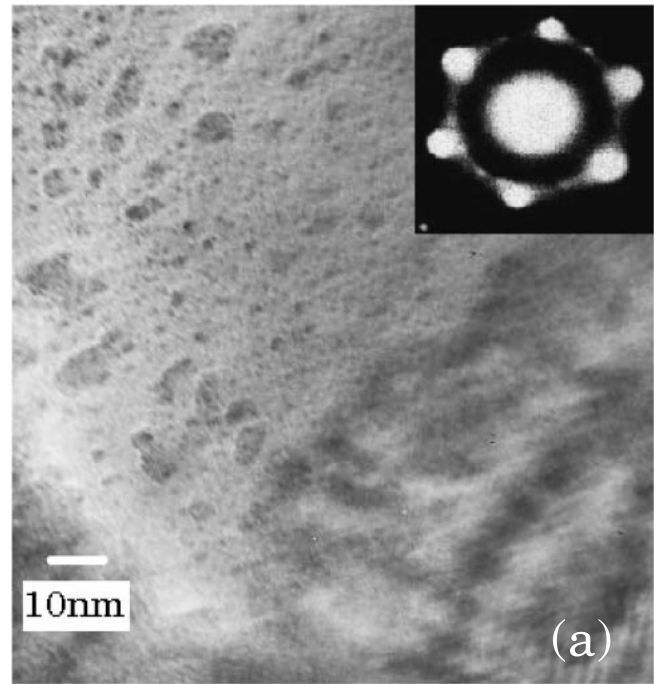

Fig. 11   (a) TEM image and (b) grain size distribution observed for the a-$Zr_{60}Cu_{30}Al_{10}$ specimen which showed $\Delta R/R_0$ of $+0.01$ due to electropulsing at RT [see TEM-2 in Fig. 8(a)].

c-Zr_2Cu is a major crystalline phase.[28] In the specimens which showed a decrease in R by electropulsing at RT or in LN_2, the major crystalline phase was c-Zr_2Cu. In contrast, the major crystalline phase was c-Zr_5Al_3 for the specimens which showed an increase in R by electropulsing. Figure 10(a) shows a TEM image observed for the a-$Zr_{60}Cu_{30}Al_{10}$ specimen which showed a decrease in R by electropulsing at RT. The inset is the SAD pattern of the whole area shown in Fig. 10(a), indicating that crystallographic directions of most crystallites (c-Zr_2Cu) showed good alignment among the crystallites. Figure 10(b) is the grain size distribution seen in Fig. 10(a), where the grain size was less than 8 nm. Figure 11(a) shows a TEM image and the SAD pattern observed for the a-$Zr_{60}Cu_{30}Al_{10}$ specimen which showed an increase in R by electropulsing at RT, indicating that crystallographic directions of most crystallites (c-Zr_5Al_3) showed good alignment among the crystallites. Figure 11(b) is the grain size distribution seen in Fig. 11(a),

where the grain size was less than 10 nm. The outline of the XRD Laue pattern observed for the a-$Zr_{60}Cu_{30}Al_{10}$ after the e-LTC were similar to that mentioned in Fig. 3(c) except that no visible XRD spots were observed (not shown here).

Figures 12(a) and (b) are similar to Fig. 4(a) and (b), respectively, but here the data observed for a-$Zr_{60}Cu_{30}Al_{10}$ are shown. In Fig. 12(a), the $i_{d0,c}$ data 1 and 3 were found in the specimens which showed a decrease in R for $\tau > 6$ ms and $\tau < 1.5$ ms and the $i_{d0,c}$ data 2 were observed for the specimens which showed an increase in R for τ between 1.5 and 6 ms, respectively. In the present τ range between 0.05 and 20 ms, $i_{d0,c}$ showed the tendency of decrease with increasing τ accompanied with the shallow minima depicted as the curves 1, 2 and 3. The dependence of $i_{d0,c}$ on τ observed for electropulsing in LN_2 was very similar to that for electropulsing at RT. Figure 12(b) shows E_d as a function of $1/2\pi f$. E_d was considerably lower than E_s. The curves 1 to 4 will be mentioned later.
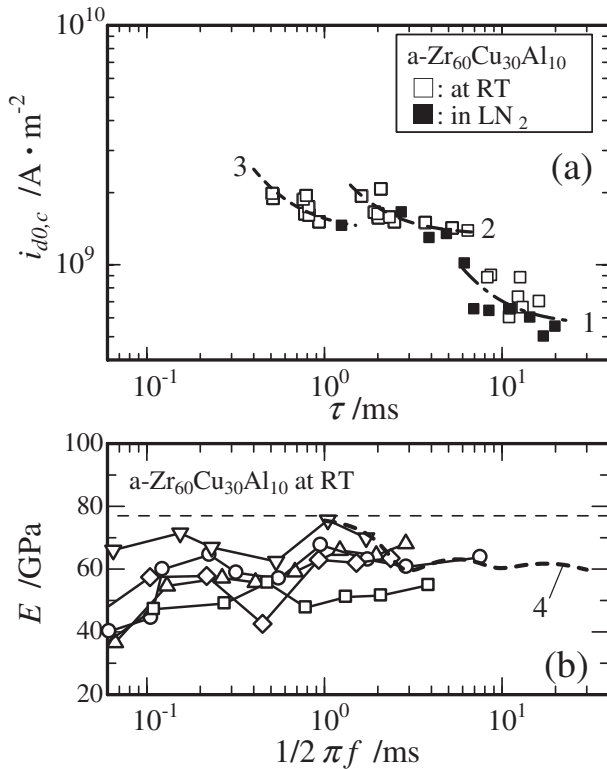
Fig. 12 (a) The $i_{d0,c}$ vs. τ data observed for electropulsing at *RT* and those observed for electropulsing in LN$_2$, where the data at *RT* reported for τ shorter than 3 ms[27] are shown too. The data 1 and 3 for $\Delta R < 0$ and the data 2 for $\Delta R > 0$. (b) The E_d vs. f data reported for a-Zr$_{60}$Cu$_{30}$Al$_{10}$ at *RT*.[19] The dashed line denotes E_s. See text for the curves 1 to 4.

4. Discussion

Nanocrystallization of amorphous alloys at ambient temperatures has been found for the deformation-induced crystallization too.[29,30] For the deformation-induced crystallization, no alignment of crystallographic directions of crystallites has been reported and it has been claimed that plastic-deformation-assisted atomic transport is responsible for the precipitation of nanocrystallites. A computer simulation work on plastic deformation of metallic glass[16] has shown that the amorphous structure is composed of the relatively lower dense region and the relatively higher dense region and the enhancement of diffusional mobility takes place in inside of deforming shear bands associated with relatively low density region. The deformation-induced crystallization[28,29] may be understood as one kind of the thermal-crystallization.

In the present work, it was commonly found for marginal amorphous alloys, a-Cu$_{50}$Ti$_{50}$ and a-Pd$_{80}$Si$_{20}$, and a bulk amorphous alloy, a-Zr$_{60}$Cu$_{30}$Al$_{10}$, that single electropulsing in LN$_2$ induced the crystallization of a considerable fractional volume of the specimen when i_{d0} was increased beyond $i_{d0,c}$. The combination of the specimen temperature versus elapsed time data observed during electropulsing in LN$_2$ or that at *RT* and the TTT diagrams[21,27] indicates that no detectable thermal-crystallization is expected during the present single electropulsing. On the other hand, a collective motion of the relatively high density region may possibly bring about diffusional motions in the relatively low density

region around the relatively high density region, resulting in the thermal-crystallization in the relatively low density region. In this model, no alignment of crystallographic directions of crystallites is expected as mentioned for the deformation-induced crystallization. In this model, however, no detectable thermal-crystallization is expected because of a very short elapsed time. Then one can say that the *e*-LTC is associated with the crystallization of the relatively high density region due to an athermal process.

In a melt spun amorphous alloy, the density fluctuation may be composed of that quenched at T_g and the additional density fluctuation expected at ambient temperature in the *a*-solid. Therefore, the latter is expected to be much smaller than the density fluctuation quenched in T_g. The present result supports this point of view, because the $i_{d0,c}$ vs. τ data observed for electropulsing in LN$_2$ showed good agreement with those observed for electropulsing at *RT*.

A possible mechanism for the aligned crystallization is a transformation of the relatively high density region to a crystalline phase. Since the synchronized cooperative motion of all atoms in the relatively high density region does not modify the local atomic configuration in the relatively high density region, such cooperative motion cannot induce the structural transformation of the amorphous structure into the crystalline structure. It is known that for the electromigration effect, the effective charge number, z^*, of a single atom is a function of atomic species[20] as well as the atomic mass. Thus, it is expected that the amplitude of displacement during the collective motion is a function of atomic species, resulting in the modification of the local atomic configuration in the relatively high density region. When the modified local atomic structure and chemical composition in the relatively high density region are inside in the permissible ranges for the crystalline phase formed, the transformation of the relatively high density region to the crystalline phase may be expected. In this model, the size of the crystallites formed during the *e*-LTC is governed not only by the size of the relatively high density region but also by the chemical composition of the relatively high density region.

For a-Cu$_{50}$Ti$_{50}$, the maximum change of R/R_0 associated with the *e*-LTC due to single electropulsing at *RT* was 0.5 in $|\Delta R/R_0|_{r\text{-}e}/|\Delta R/R_0|_x$ and the size of crystallites formed during the *e*-LTC was about 10 nm for most crystallites and several tens nm as a maximum after the *e*-LTC with τ of 6.3 ms. The visible XRD Laue spots suggest that whether they reflect the maximum size of an aligned crystallized region or the size of a crystallite. These results suggest that the modified atomic structure and chemical composition of the relatively high density region during the *e*-LTC was inside in the permissible range of *c*-CuTi as the most case. The observation of Debye rings and the correlation of the width of the Debye rings with the direction of electric current suggest that the direction of aligned crystallization is a function of both the direction of electric current and the internal stress.

For a-Pd$_{80}$Si$_{20}$, crystalline phases formed by the *e*-LTC[21] were *c*-Pd$_3$Si, *c*-Pd$_9$Si$_2$ and fcc-Pd(Si) which were observed after the thermal crystallization[31] and the unknown crystalline phase. The maximum decrease in R/R_0 associated with the *e*-LTC during single electropulsing was 0.35 in $|\Delta R/$

$R_0|_{\text{r-e}}/|\Delta R/R_0|_x$ and the size of crystallites formed during the e-LTC was 2 to 5 nm for most crystallites. These results suggest that the relatively high density regions in a-Pd$_{80}$Si$_{20}$ are mainly composed of those with the amorphous structure and the chemical composition favorable to c-Pd$_3$Si, c-Pd$_9$Si$_2$, fcc-Pd(Si) and the unknown phase and the size of such relatively high density regions may be 2 to 5 nm as the most case.

For a-Zr$_{60}$Cu$_{30}$Al$_{10}$, the maximum decrease in $|\Delta R/R_0|_{\text{r-e}}/|\Delta R/R_0|_x$ after the e-LTC due to single electropulsing was 0.05, indicating that the amorphous structure and/or the chemical composition of most of the relatively high density regions are not near of a probable crystalline phase. For the remaining relatively high density regions, the e-LTC for $\tau > 6$ ms and $\tau < 1.5$ ms caused the decrease in R and the formation of c-Zr$_2$Cu which were observed for the thermal crystallization at elevated temperature. The size of crystallites was less than 8 nm. On the other hand, the e-LTC for τ between 6 ms and 1.5 ms caused the increase in R, where the major crystalline phase was c-Zr$_5$Al$_3$ and the size of most crystallites was less than 2 nm. These results suggest that in a-Zr$_{60}$Cu$_{30}$Al$_{10}$, the relatively high density regions associated with the e-LTC are composed of the relatively high density regions with the amorphous structure and the chemical composition favorable to c-Zr$_2$Cu and those favorable to c-Zr$_5$Al$_3$, where the size of relatively high density regions may be a function of their chemical composition.

As mentioned in the section 1, it is suggested that a resonant collective motion of many atoms can be excited by elastic vibration resulting in the decrease in the dynamic Young's modulus observed. In the present work, such resonant collective motion of many atoms may be excited by resonant electropulsing resulting in the e-LTC. If it is the case, a close correlation between the $i_{d0,c}$ *vs.* τ data observed for the e-LTC and the E_d *vs.* f data observed for the dynamic elastic response will be expected. For the forced vibration of resonant systems with the mass, m, the dependence of the displacement amplitude, x_0, on the angular frequency, ω, can be given by

$$x_0^2 = (F_0/m)^2/[(\omega^2 - \omega_r^2)^2 + \omega_r^4 \tan^2 \phi], \qquad (2)$$

where F_0 is the strength of a periodic applied force, ω_r is the resonant angular frequency and ϕ is the loss angle.[32] For the resonant collective motion of the relatively high density region excited by electropulsing, we assume that F_0 is proportional to i_{d0}, ω can be replaced by $1/\tau$, and the e-LTC takes place when x_0 is increased beyond the threshold value. Then, one may have the following equation

$$i_{d0,c} = \alpha[(1/\tau^2 - 1/\tau_r^2)^2 + \tan^2 \phi/\tau_r^4]^{1/2} + (i_{d0,c})_s, \quad (3)$$

where α is a proportional constant and $(i_{d0,c})_s$ is a function of the threshold value of x_0. For the elasticity measurement, we assume that the anelastic strain associated with the resonant collective motions, ε_a, is explained by,

$$\varepsilon_a = \beta/[(\omega^2 - \omega_r^2)^2 + \omega_r^4 \tan^2 \phi]^{1/2}, \qquad (4)$$

and E_d is given by,

$$E_d = E_s[\varepsilon_0/(\varepsilon_0 + \varepsilon_a)], \qquad (5)$$

where ε_0 is the elastic strain and β is a proportional constant. For the resonant collective motion of relatively high density region, $\tan \phi$ may be considerably large because the relatively high density region is embedded in the relatively low density region. For such case, both the dependence of $i_{d0,c}$ on τ and the dependence of ε_a on ω are not strongly modified by a change in $\tan \phi$. In the following, $\tan^2 \phi$ will be assumed to be 0.5.

For a-Cu$_{50}$Ti$_{50}$, in Fig. 4(a), the theoretical curves 1 to 3 estimated by using eq. (3) are fitted to the $i_{d0,c}$ *vs.* τ data, where τ_r assumed is 35, 4 and 0.4 ms for the curves 1, 2 and 3, respectively. It is noted that with decreasing τ, the theoretical $i_{d0,c}$ *vs.* τ curve shows a shallow minimum at $\tau = \tau_r$ and then a steep increase. In Fig. 4(b), the theoretical curve 4 estimated by using eqs. (4) and (5) and τ_r assumed for the curves 1 to 3 is fitted to the E_d *vs.* $1/2\pi f$ data. It is noted that the theoretical E_d *vs.* $1/2\pi f$ curve shows a shallow minimum at $\tau = \tau_r$. The curves 1 to 3 explain the outline of the $i_{d0,c}$ *vs.* τ data and the curve 4 explains the outline of the E_d *vs.* $1/2\pi f$ data, respectively. The present result supports the point of view that the resonant collective motion of the relatively high density region is responsible for the e-LTC and the softening of E_d. It is also indicated that the size distribution of relatively high density region in a-Cu$_{50}$Ti$_{50}$ was not continuous but discrete. The observed result that the maximum change of R/R_0 due to single electropulsing was 0.5 in $|\Delta R/R_0|_{\text{r-e}}/|\Delta R/R_0|_x$ indicates that most of the relatively high density regions in a-Cu$_{50}$Ti$_{50}$ have the local amorphous structures and chemical compositions being inside in the permissible ranges for c-CuTi.

For a-Pd$_{80}$Si$_{20}$, in Fig. 7(a), the theoretical curves 1 and 2 are fitted to the $i_{d0,c}$ *vs.* τ data, where τ_r assumed is 25 and 2 ms for the curves 1 and 2, respectively. In Fig. 7(b), the theoretical curve 3 is fitted to the E_d *vs.* $1/2\pi f$ data by using τ_r assumed for the curves 1 and 2. The curves 1 and 2 explain the outline of the $i_{d0,c}$ *vs.* τ data and the curve 3 appears to explain the E_d *vs.* $1/2\pi f$ data. Since crystalline phases formed by the e-LTC were c-Pd$_3$Si, c-Pd$_9$Si$_2$, fcc-Pd(Si) and the unknown phase, various kinds of relatively high density regions favorable to these crystalline phases may exist in a-Pd$_{80}$Si$_{20}$. On the other hand, the $i_{d0,c}$ *vs.* τ data for these various kinds of relatively high density regions were very similar to each other, indicating that their size distributions were similar to each other too.

For a-Zr$_{60}$Cu$_{30}$Al$_{10}$, in Fig. 12(a), the theoretical curves 1 to 3 are fitted to the $i_{d0,c}$ *vs.* τ data, where τ_r assumed is 35 ms, 10 ms and 3 ms for the curves 1 to 3, respectively. It is noted that the curves 1 and 3 are fitted to the e-LTC inducing c-Zr$_2$Cu which is the major crystalline phase observed after the thermal crystallization and that the curve 2 is fitted to the e-LTC inducing c-Zr$_5$Al$_3$. In Fig. 12(b), the theoretical curve 4 is estimated by using τ_r assumed for the curves 1 to 3. Since the maximum change in $|\Delta R/R_0|_{\text{r-e}}/|\Delta R/R_0|_x$ due to single electropulsing is 0.05, the fractional volume ratio of the relatively high density regions favorable to c-Zr$_2$Cu and c-Zr$_5$Al$_3$ may be considerably low. It is indicated that one of the reasons for the high thermal stability of a bulk amorphous alloy, a-Zr$_{60}$Cu$_{30}$Al$_{10}$, is the low fractional volume ratio of the relatively high density regions favorable to crystalline phases.

5. Conclusion

The e-LTC was studied for a-Cu$_{50}$Ti$_{50}$, a-Pd$_{80}$Si$_{20}$ and a-Zr$_{60}$Cu$_{30}$Al$_{10}$ by means of electropulsing in LN$_2$ and that at RT, indicating that the density fluctuation responsible for the e-LTC was that frozen at T_g. The crystallographic direction of crystallites formed by the e-LTC showed good alignment among the crystallites, indicating that the resonant collective motion of the relatively high density region causes the transformation from an amorphous structure to a crystalline structure in the relatively high density region. The maximum change in $|\Delta R/R_0|_{r\text{-}e}/|\Delta R/R_0|_x$ due to single electropulsing was 0.5, 0.35 and 0.05 for a-Cu$_{50}$Ti$_{50}$, a-Pd$_{80}$Si$_{20}$ and a-Zr$_{60}$Cu$_{30}$Al$_{10}$, respectively. indicating that the fractional volume ratio of the relatively high density regions favorable to crystalline phase(s) decreases in the order of a-Cu$_{50}$Ti$_{50}$, a-Pd$_{80}$Si$_{20}$ and a-Zr$_{60}$Cu$_{30}$Al$_{10}$. A probable mechanism for the e-LTC was discussed.

Acknowledgement

REFERENCES

1) H. Mizubayashi and S. Okuda: Phys. Rev. B **40** (1989) 8057–8060.
2) Z. H. Lai, H. Conrad, Y. S. Chao, S. Q. Wang and J. Sun: Scr. Metall. **23** (1989) 305–310.
3) H. Conrad: Mater. Sci. Eng. A **287** (2000) 227–237.
4) H. Mizubayashi and R. Takemoto: Defect and Diffusion Forum **95–98** (1993) 1187–1192.
5) R. Takemoto and H. Mizubayashi: Mater. Sci. Engng. A **179/180** (1994) 275–278.
6) R. Takemoto and H. Mizubayashi: Acta Metall. Mater. **43** (1995) 1495–1504.
7) R. Takemoto, M. Nagata and H. Mizubayashi: Acta Metall. Mater. **44** (1996) 2787–2795.
8) G.-Q. Teng, Y. Chao, L. Dong, Y. Geng and Z. Lai: Jpn. J. Appl. Phys. **35** (1996) 5320–5325.
9) Z. H. Lai, H. Conrad, G. Q. Teng and Y. S. Chao: Mater. Sci. Eng. A **287** (2000) 238–247.
10) Y. Dolinsky and T. Elperin: Phys. Rev. B **58** (1998) 3008–3014.
11) R. S. Qin, S. X. Su, J. D. Guo, G. H. He and B. L. Zhou: Nanostr. Mater. **10** (1998) 71–76.
12) Y. Dolinsky and T. Elperin, Phys. Rev. B **68** (2003) 026101.
13) H. Mizubayashi, T. Okamoto, K. Koyama and M. Horiuchi: Acta Mater. **46** (1998) 1257–1264.
14) H. Mizubayashi, T. Usui and H. Tanimoto: J. Non-Cryst. Solids **312–314** (2002) 542–546.
15) D. Weaire, M. F. Ashby, J. Logan and M. J. Weins: Acta Metall. **19** (1971) 779–788.
16) S. Takeuchi and K. Maeda: Key Eng. Mater. **13/15** (1987) 749–760.
17) Y. Suzuki, J. Haimovich and T. Egami: Phys. Rev. B **35** (1987) 2162–2168.
18) H. Mizubayashi and R. Takemoto: J. Alloys Comp. **211/212** (1994) 340–343.
19) H. Mizubayashi, T. Usui and H. Tanimoto: Mater. Sci. Eng. A **370** (2004) 260–263.
20) H. B. Huntington, *Diffusion in Solids*, ed. A. S. Nowic and J. J. Burton (Academic Press, New York, 1975), p. 303.
21) H. Mizubayashi, N. Kameyama, T. Hao and H. Tanimoto: Phys. Rev. B **64** (2001) 054201.
22) T. Ichitsubo, S. Kai, H. Ogi, M. Hirao and K. Tanaka: Scr. Mater. **49** (2003) 267–271.
23) T. Ichitsubo, E. Matsubara, S. Kai and M. Hirao: Acta Mater. **52** (2004) 423–429.
24) T. Ichitsubo, E. Matsubara, K. Anazawa, N. Nishiyama, S. Kai and M. Hirao: Mater. Trans., JIM **45** (2004) 1189–1193.
25) A. Inoue: Acta Mater. **48** (2000) 279–306.
26) M. Yamasaki, S. Kagao and Y. Kawamura: Scr. Mater. **53** (2003) 63.
27) H. Mizubayashi, T. Hao and H. Tanimoto: J. Non-Cryst. Solids **312–314** (2002) 581–584.
28) C. Fang, A. Takeuchi and A. Inoue: Mater. Trans., JIM **40** (1999) 42–51.
29) J. J. Kim, Y. Choi, S. Suresh and A. S. Argon: Science **295** (2002) 654–657.
30) W. H. Jiang, F. E. Pinkerton and N. Atzmon: J. Appl. Phys. **93** (2003) 9287–9290.
31) T. Masumoto and R. Maddin: Acta Melall. **19** (1971) 725–741.
32) A. S. Nowick and B. S. Berry: *Anelastic Relaxation in Crystalline Solids* (Academic Press, New York and London, 1972), p. 15.